Mechanism of Proton Entry into the Cytoplasmic Section of the Proton-Conducting Channel of Bacteriorhodopsin †

ARTICLE *in* BIOCHEMISTRY · DECEMBER 1997

Impact Factor: 3.02 · DOI: 10.1021/bi9717542 · Source: PubMed

4 AUTHORS, INCLUDING:

Esther Nachliel
Tel Aviv University
104 PUBLICATIONS **2,147** CITATIONS
SEE PROFILE

Norbert A Dencher
Technical University Darmstadt
178 PUBLICATIONS **7,229** CITATIONS
SEE PROFILE

Menachem Gutman
Tel Aviv University
181 PUBLICATIONS **3,635** CITATIONS
SEE PROFILE

Mechanism of Proton Entry into the Cytoplasmic Section of the Proton-Conducting Channel of Bacteriorhodopsin†

Sharon Checover,‡ Esther Nachliel,*,‡ Norbert A. Dencher,§ and Menachem Gutman‡

Laser laboratory for Fast Reactions in Biological Systems, Department of Biochemistry, Tel Aviv University, Tel Aviv 69978, Israel, and Institute of Biochemistry, Technische Hochschule Darmstadt, Petersenstrasse 22, D-64287 Darmstadt, Germany

Received July 18, 1997; Revised Manuscript Received August 28, 1997⊗

ABSTRACT: Bacteriorhodopsin is the light-driven proton-pumping protein of *Halobacterium salinarum* that extracts protons from the well-buffered cytoplasmic space within the time limits set by the photocycle turnover. The specific mechanism of the proton uptake by the cytoplasmic surface of the protein was investigated in this study by the laser-induced proton pulse technique. The purple membrane preparations were labeled by fluorescein at two residues (36 or 38) of the cytoplasmic surface of the protein, sites that are close to the orifice of the proton-conducting channel. The membranes were pulsed by protons discharged from photoexcited pyranine [Nachliel, E., Gutman, M., Kiryati, S., and Dencher, N. A. (1996) *Proc. Nat Acad. Sci. U.S.A.* 93, 10747−10752). The reaction of the discharged protons with the pyranine anion and the fluorescein was measured with sub-microsecond resolution. The experimental signals were reconstructed through numeric integration of differential rate equations which quantitated the rates of all proton transfer reactions between all reactants present in the system. The interaction of protons with the orifice of the cytoplasmic channel is enhanced by the exposed carboxylates of the protein. A cluster of three carboxylates acts as a strong proton attractor site while one carboxylate, identified as D36, acts as a mediator that delivers the proton to the channel. The combination of these reactions render the surface of the protein with properties of a proton-collecting antenna. The size of the collecting area is less than that of the protein's surface.

The structure of the intramembranal section of bacteriorhodopsin (BR)[1] is well established (*1*−*3*), yet, due to the flexibility of the loops connecting the transmembrane helices, the organization of the amino acid residues at the protein/water interface is not fully resolved. In this study we monitor, by time-resolved kinetics, the interaction of protons with the groups on the protein's surface and deduce the functional organization of the proton reactive moieties. On the basis of these measurements, we deduce how the surface supports the physiological function of the protein.

Under physiological conditions the cytoplasmic (CP) surface of the protein has to pick up protons from the well-buffered, neutral pH cytoplasmic matrix. For efficient functioning, the protein must bind protons and retain them for a time frame comparable with the reprotonation time of D96 (5−10 ms). To attain this kinetic competence the protein is assisted by the negatively charged head groups of the lipids interspaced between the BR molecules (*4*−*6*) and the carboxylates of the protein itself (*7*−*10*).

The rate of proton transfer between sites that which are very close to each other is extremely sensitive to the distance and the angle between them (*11*−*14*). Consequently, even marginal transient motion of carboxylates on the surface, one with respect to the other, will modulate the probability of proton transfer between them. Such structural transients can provide a proton-collecting surface with an efficient mechanism for preferential delivery of protons toward the orifice of the protonic channel. Consequently, the detection of temporary bridging structures has to rely on dynamic measurements of proton transfer between the bulk of the solution and the orifice of the channel. In these measurements the participation of the surface groups and their contribution to the effective flux of protons toward the orifice can be quantitated. Such experiments had been carried out by the application of the laser-induced proton pulse (*15*). The measurements are based on the synchronized release of protons from a water soluble molecule, pyranine, that due to its negative charges is not adsorbed to the purple membranes. The dye is excited by a short laser pulse which shifts the pK of the dye from p$K_0 = 7.7$ down to p$K^* = 1.4$ and the proton dissociates from the excited molecule with a time constant of $\tau = 120$ ps (*16*). After the relaxation of the excited anion to the ground state ($\tau = 6$ ns) it regains its high pK, but the excessive dissociation in the excited state poised the system in a temporary state of disequilibrium. The discharged protons react in a diffusion-controlled reaction with all of the components present in the system. The velocity of the reaction with each protonatable moiety is in accordance with its concentration, charge, and availability to the bulk. Following the perturbation, the system

† Part of the research is supported by the Deutsche Forschungsgemeinschaft SFB 472 and the Fonds der Chemischen Industrie (N.A.D.).

* To whom correspondence should be addressed.

‡ Tel Aviv University.

§ Technische Hochschule Darmstadt.

⊗ Abstract published in *Advance ACS Abstracts,* October 15, 1997.

[1] Abbreviations: BO_{36}, BO_{38}, bacterioopsin labeled with fluorescein on its 36th or 38th residue, respectively. BR_{36}, BR_{38}, bacteriorhodopsin labeled with fluorescein on its 36th or 38th residue, respectively. ΦOH, ΦO^-, pyranine (8-hydroxy-1,3,6-pyrenetrisulfonate) in its protonated and deprotonated states, respectively; Flu, fluorescein; CP and EC are the cytoplasmic and extracellular surfaces of the purple membrane, respectively.

S0006-2960(97)01754-6 CCC: $14.00

relaxes to the prepulse state. The dynamics of the relaxation are determined to a large extent by the p*K* values of the sites that were protonated; a compound with p*K* of 4 will retain a proton for less than a microsecond, while those with p*K* = 7 will retain a proton for ~500 ms (*12*). Because of this free energy correlation the dynamics of pyranine anion's reprotonation are modulated by the p*K* values of each of the present reactants. In simple cases, it is possible to deduce from these observations the dynamic and thermodynamic characteristics of the reactants (*17*). However, when a second indicator is covalently attached to the surface under study, much more refined information can be obtained (*15*, *18*). The simultaneous monitoring of the state of protonation of the two chromophores allows us to calculate the rate constants of protonation of all reacting groups, their p*K* values, and how fast they can exchange a proton among themselves.

In a previous study, we employed this method for quantitation of the proton reactions with the EC side of purple membrane (*15*). Two types of membrane preparations were investigated: native purple membranes, which were labeled on their EC side by fluorescein molecule attached to the ϵ-amine moiety of lysine 129, and membranes made with the retinal-devoid protein (BO), which were labeled at the same position. The experiments indicated that the EC face of the protein, either BR or BO, bears only one carboxylate that, within the time frame of our observation (less than 1 ms), is actively involved in reversible proton binding. On the CP face of the membrane we found two to five protonable moieties: the BO samples contains only two to three protonable sites on the CP face, while the photoreactive purple membranes had four to five carboxylates which were found to be very efficient in picking up protons from the solution. The reaction of these groups with protons in bulk was so fast that it appeared as if they formed a cluster in which the charge of one assists the protonation of the other (*15*).

In the present study we introduced the fluorescein probe on the CP surface at two different sites. In one case the probe was attached to the 38th position of the protein (using the D38C mutant), which is in the orifice of the protonic channel (*8*). In the other case, the fluorescein was linked to the 36th position (D36C) which is on the short loop connecting helices A and B. Each preparation was studied both in its retinal-devoid form (BO_{36} and BO_{38}) and in its native form (BR_{36} and BR_{38}). The advantage of having a reporter close to the site of action increased the resolution of the kinetic analysis so that a clear discrimination between the various carboxylate of the CP side could be obtained.

MATERIALS AND METHODS

Derivatization of Thiol Groups in Cysteine-Containing Bacteriorhodopsin Mutants with Fluorescein-5-maleimide

Site-specific Cys-mutants of bacteriorhodopsin, D36C and D38C, were prepared according to Ferrando et al. (*19*). Mutated proteins were isolated as purple membrane sheets. A spectroscopic and functional characterization of D36C and D38C bacteriorhodopsin is given in Riesle et al. (*8*). Protein lacking the chromophore retinal, i.e., bacterioopsin (BO), was prepared by illumination of mutant BR in the presence of hydroxylammonium chloride as described in Nachliel et al. (*15*). Thereafter, the retinaloxime that formed and was residing in the membrane was removed completely by a bovine serum albumin washing procedure.

Selective labeling of Cys 36 and Cys 38, respectively, in BR and BO was achieved using fluorescein-5-maleimide according to Heberle et al. (*20*). The Cys-mutant protein in the membrane sheets (53 μM) was preincubated with 160 μM dithiothreitol in the presence of 1 mM EDTA, 150 mM KCl, and 20 mM sodium phosphate buffer at pH 6.9 and 20 °C with stirring under an argon atmosphere for 70 min. Thereafter, the sample was treated with 1.6 mM fluorescein-5-maleimide dissolved in dimethylformamide (final concentration of 2.5%) under argon in the dark for 15 h, followed by washing with 150 mM KCl (five times) and dialysis. The labeling efficiency was determined from the absorption spectra of the samples and found to be 42%, 51%, 42%, and 35% for the BO_{36}, BO_{38}, BR_{36}, and BR_{38}, respectively.

Kinetic Measurements of Proton Transfer between Bulk and Membrane

The purple membranes were suspended in 750−800 μL (final volume) of 1−2 mM NaCl containing 10−30 μM pyranine. The sample, placed in a four-face quartz cuvette (1 cm × 1 cm), was constantly stirred by a magnetic bar while the pH was monitored by a glass electrode. The excitation beam (Nd:Yag laser, (λ = 335 nm, 2 ns FWHM, 1.6 mJ/pulse, 10 Hz) excited the full width of the cuvette, and the transient absorbencies, following the excitation pulse, were monitored by a probing beam of an Ar laser (496 and 458 nm for fluorescein and pyranine, respectively) that crossed the cell perpendicular to the excitation beam. The signals were collected by a Tektronix digital oscilloscope (TDS-540A) and averaged. For more details see Nachliel et al. (*15*).

Kinetic Analysis of the Absorbance Transients

The absorbance transients were converted to molar concentration using differential (alkaline minus acidic) extinction coefficients of fluorescein (50 000 M^{-1} cm^{-1}, 496 nm) and the pyranine (24 000 M^{-1} cm^{-1}, 458 nm). The concentration transients of the fluorescein and the pyranine were also adjusted for the spectral contributions of one at the wavelength where the other was measured.

The simulation of the dynamics was carried out as described in our previous paper (*15*). Each group on the surface of the protein, that can interact with proton within the observation time, is explicitly defined by a set of rate constants. These groups are given in the model presented by Scheme 1. The participating reactants are the proton emitter (ΦOH) which is present on both sides of the membrane, the various carboxylates (COO^-) which are present in unequal quantities on each side of the membrane, and the covalently bound fluorescein (Flu^-). The EC side of the protein is represented by a single carboxylate while the CP surface carries two to five carboxylates (depending on the nature of the preparation, BR or BO; *15*). As the efficiency of labeling was 30−50%, the unlabeled fraction was represented in the calculations by its full quota of carboxylates. The unlabeled protein is referred to in the tables as COO^-_0.

To convert the multiequilibria system into a kinetic model, all of the reactions were combined into a set of coupled,

Scheme 1

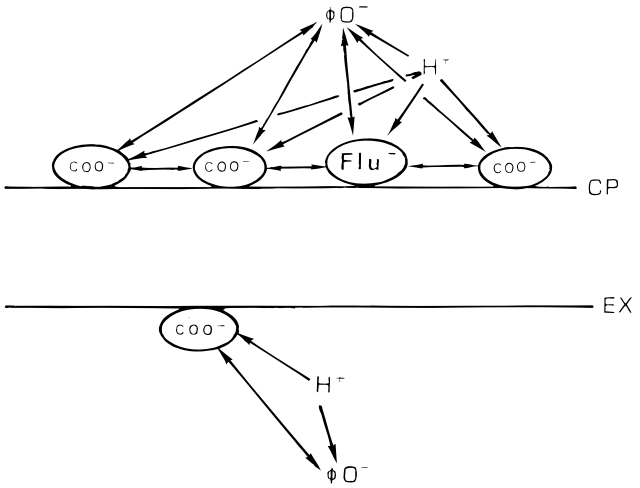

nonlinear, parametric differential rate equations which complied with the detailed balance principle. A perturbation was introduced as an increment of the pyranine anion and the free proton concentrations (the concentration of the undissociated pyranine was reduced by the same magnitude). The perturbation was propagated to the other reactants by the reactions indicated by the arrows in Scheme 1. The dimensions of the rate constants are M^{-1} s^{-1} or s^{-1}, depending on the order of the reaction. In these reactions in which one of the reactants was a free diffusing molecule, the rate constants are of diffusion-controlled second-order reactions. In reactions in which a proton is exchanged between moieties that are fixed on the surface of the protein, we utilized the mechanism of a *virtual second-order reaction*; the reactants exchange a proton among themselves as if they can collide with each other. A detailed description of the model is given in ref (*14*). The rate constants of the virtual second-order reactions have no direct physical meaning, yet their values are suitable for comparative purposes. The differential equations were integrated numerically using the rate constants as adjustable parameters. Each pair of signals (pyranine and fluorescein signals) measured for the same value of initial conditions was simulated by solving the differential rate equations. An acceptable solution was a set of rate constants that reproduce the measured dynamics within the boundaries set by the electronic noise of the measuring system. The same procedure was repeated for all tracing gathered for each preparation as measured under varying initial conditions (pH, concentration of reactants) looking for this set of constants that will reconstruct the dynamics irrespective of the specific initial conditions (for details and elaboration on the method see refs 17, 21, and 22).

The number of reacting moieties per protein was taken as measured before (*15*). The strategy in the assignment of the p*K* values was to allocate for all carboxylates the same p*K* values and kinetic rate constants that are similar to those measured for the BR preparations labeled by fluorescein on the EC side (*15*). Yet, due to the higher resolution gained by the introduction of fluorescein on the cytoplasmic side of the membrane, these parameters were insufficient for the reconstruction of the dynamics. Consequently the various surface groups were allowed to diverge in their properties, while keeping the complexity of the system (the number of nonidentical moieties) to a minimum. The solution given in this publication is the simplest one that could reconstruct all of the measured transients.

Table 1: p*K* Values of Fluorescein Attached to BR Preparations at Low and High Ionic Strength

	p*K*			
	$I < 10^{-4}$ M	$I \geq 0.4$ M	σ ($e^-/Å^2$)	charge/protein
Flu−BO_{36}	8.18 ± 0.055	7.51 ± 0.19	3.3×10^{-4}	−0.38[a]
Flu−BO_{38}	7.98 ± 0.05	7.47 ± 0.05	3.0×10^{-4}	−0.34
Flu−BR_{36}	8.58 ± 0.11	7.47 ± 0.03	4.1×10^{-4}	−0.47
Flu−BR_{38}	8.15 ± 0.05	7.49 ± 0.01	4.1×10^{-4}	−0.47
Flu (free)	6.60 ± 0.05	6.32 ± 0.05	−	−
Flu−BR_{129}[b]	8.40 ± 0.05	7.30 ± 0.05	8.2×10^{-4}	−0.94

[a] The surface area of the protein on its cytoplasmic side was taken as 1150 $Å^2$. [b] The value is taken from Nachliel et al. (*9*).

RESULTS

pH Titration of the Bound Fluorescein

Spectrophotomtric titrations of the fluorescein attached to either the 38th or 36th position, both for the BO and the BR preparations, were carried out in solutions of varying ionic strength. In these titrations we took care to correct for the slow reversible formation of the bleached tautomer of fluorescein molecule that appears upon the protonation of the dye's carboxylate. The resulting p*K* values of the four preparations are listed in Table 1.

The dye, when bound to the membrane, exhibits a large p*K* shift with respect to its free form. Part of the shift is due to the local hydrophobicity, as evident from the p*K* values measured at ionic strengths higher than 0.4 M. The other cause for the p*K* shift is the electrostatic potential. From the dependence of the p*K* on the ionic strength we calculated the charge density (σ) and the total charge per BR molecule based on a surface area of 1150 $Å^2$ per protein (*23*).

The membrane carries a large number of sulfonated glycolipids and phospholipids. Due to the low p*K* of these groups they cannot retain a proton for more than a fraction of a microsecond. Some of the protein's carboxylates may have a partial accessibility to the bulk. These carboxylates will hardly be protonated within the few microseconds that the free proton concentration is above the equilibrium level. As a result, not all carboxylates are detectable in the kinetic experiments.

Kinetics of Protonation of Fluorescein Bound to the CP Side of Purple Membranes

Typical results of a proton pulse experiment are given in Figure 1. An aqueous solution of pyranine together with fluorescein was irradiated by a train of laser pulses, and the absorption transients after each pulse were measured and averaged. In this figure we present results obtained either with the free fluorescein (curves A and B) or with the dye bound to the 36th position of a BO preparation (curves C and D). At zero time, the pyranine was excited by a laser pulse and dissociated into a free proton and pyranine anion, having a strong absorbance at 458 nm (curves A and C). The released protons interacted in a diffusion-controlled reaction with the pyranine anion, the fluorescein, and the protein (if present). The reaction with pyranine was measured by the fast decay of the absorbance at 458 nm, while the protonation of the fluorescein was monitored by the

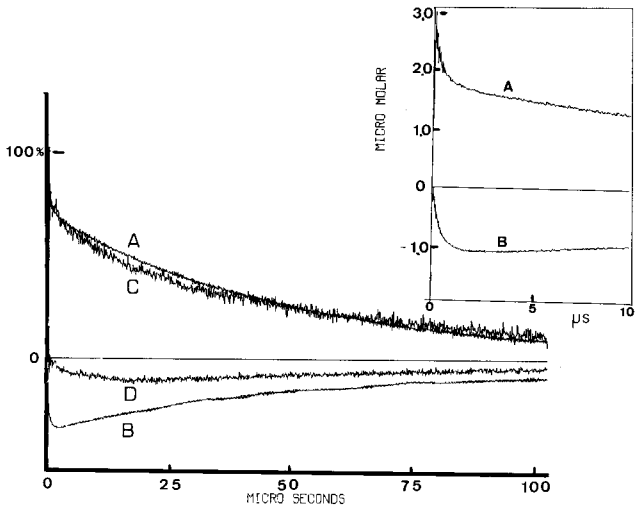

FIGURE 1: Kinetic measurements of pulse perturbation of a pyranine solution containing fluorescein. Aqueous solutions of pyranine (18.5 μM) and fluorescein (10.5 μM, pH = 7.65) were irradiated by a train of laser pulses (1.6 mJ/pulse, 355 nm, at 10 Hz), and the absorbencies were measured at 458 nm (curves A and C) and 496 nm (curves B and D). The absorption transients were converted to concentrations as described under Materials and Methods. Curves A and B were measures for the free fluorescein, while for Curves C and D, the fluorescein (10.56 μM) was bound to the 36th position of the BO preparation (25.1 μM of protein). Each pair of measurements was normalized with respect to the amount of pyranine that was dissociated by the laser pulse. In absence of protein 100% = 3.17 μM. In the presence of the BO membranes, the light scattering reduces the intensity of the laser pulse and 100% = 1.05 μM. The inset expands the tracings measured in the absence of the protein over the first 10 μs.

decrement of the absorption at 496 nm (curves B and D). There is a clear distinction between the reactions measured with free fluorescein and with fluorescein in its protein-bound state. In the absence of protein (curves A and B) both dyes react with the released protons in a diffusion-controlled reaction until all of the released protons are taken up. This phase of the reaction is shown in the inset to Figure 1, which expands the events during the first 10 μs of the reaction. The rest of the reaction is much slower, proceeding mainly through collisional proton transfer between the protonated fluorescein and the pyranine anion. The binding of the fluorescein to the BO membranes alters the magnitude and the shape of the signals. The smaller signal is attributed to the scattering of the laser pulse, which lowers the efficiency of the pulse-driven dissociation of the pyranine. The reprotonation of the pyranine anion is very similar to that measured in the absence of the protein (compare curves A and C), indicating that the buffering moieties of the membranes react with the released protons and offer fair competition with respect to the pyranine anion. The dynamics of the bound fluorescein are very different from that of the free dye (curves B and D): the reaction is stretched over the time frame in which all of the released protons are already bound to the buffering moieties on the protein. This observation is direct evidence that the protonation of the protein-bound indicator occurs not only through the reaction of the fluorescein with free protons but also through a major pathway in which the protons bound to the various carboxylates of the protein can reshuffle and migrate to the bound indicator. In the rest of this study we shall quantitate this reaction by well-defined kinetic terms.

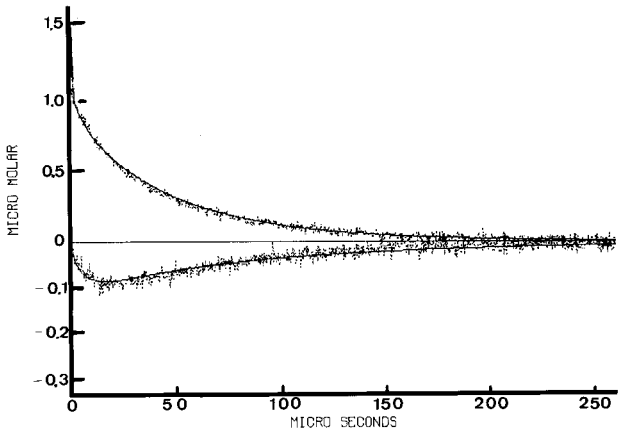

FIGURE 2: Dynamics of pulse protonation of a fluorescein-labeled BO_{38} preparation. The protein (53.7 μM containing 27.4 μM attached fluorescein) was suspended at pH = 7.2 in presence of 27.5 μM pyranine. The upper transient, of the pyranine anion, was measured at 458 nm. The lower one, of the fluorescein, was recorded at 496 nm. The experimental curves are fitted by numeric simulation using the parameters given in Table 2. For clarity, the fluorescein signal, depicted at the lower part of the figure, is drawn on an expanded scale.

The characterization of the observed dynamics in physical terms such as rate constants and pK values of the reacting moieties is attainable through the numeric analysis of the signals. A precise analysis of the dynamics calls for simultaneous reconstruction of a set of measurements that were obtained under a wide range of initial conditions. The most convenient parameter for altering these boundary conditions is the pH of the solution. Increasing the pH will enrich the prepulse concentration of the fluorescein anion and deplete the population of the proton emitter ΦOH. However, the measurements have to be conducted within a pH range where the concentration of the protonated pyranine is still high while the fluorescein is mostly in its deprotonated state. Out of this range, either the pyranine will not serve as an efficient proton emitter (pH > p$K_{\Phi OH}$) or the fluorescein will be mostly protonated, a state that is not suitable for reaction with the released protons (pH < pK_{Flu}). In the present case the range of pH that could be employed was rather narrow. The high pK values of the protein-bound fluorescein (p$K \sim 7.5-8.5$) are close to that of the pyranine molecule (p$K = 7.7$ at I $\sim 1-5$ mM). The pH range selected for the measurements ($7.1 <$ pH < 8.5) allowed the ratio of the proton donor concentration [ΦOH] to the deprotonated state of the fluorescein [Flu^-] to vary over more than 1 order of magnitude ($0.56 <$ [ΦOH]/[Flu^-] < 6.36).

Protonation of the Cytoplasmic Surface of Bacterioopsin

Figure 2 depicts the transients measured with BO_{38}. The fluorescein protonation attains its maximal value some 15 μs after the laser pulse and relaxes to the prepulse level within ~250 μs. The reaction of the pyranine anion with the protons commences with a very fast phase lasting 1−2 μs, after which velocity of the reaction slows down considerably. The slowing of the reaction corresponds with the relaxation of free protons increment to the initial prepulse level (*24*). As was found with the BO_{36} preparation, the protonation of the fluorescein on BO_{38} continues well within the time frame in which the free proton concentration already declined to a level where the reaction with the pyranine anion is in the slow regime. This implies that the protonation of

Table 2: Kinetic and Thermodynamic Characterization of Fluorescein and the Carboxylates on the Cytoplasmic Surface of the Bacterioopsin[a]

	Flu−BO_{36}			Blu−BO_{38}		
reaction	*n*	p*K*	*k*	*n*	p*K*	*k*
1. $\Phi O^- + H^+$			$(4.9 \pm 0.4) \times 10^{10}$			$(4.0 \pm 2.0) \times 10^{10}$
2. $Flu^- + H^+$			$\mathbf{(6.6 \pm 2.5) \times 10^9}$			$\mathbf{(4.0 \pm 1.9) \times 10^9}$
3. $COO^-_{EC} + H^+$	1	5.0	$(8.0 \pm 1.0) \times 10^9$	1	4.5	$(8.0 \pm 1.0) \times 10^9$
4. $COO^-_0 + H^+$	3	5.5	$(1.00 \pm 0.1) \times 10^{10}$	3	5.4	$(8.0 \pm 0.3) \times 10^9$
5. $COO^-_A + H^+$	1	5.5	$(1.7 \pm 0.5) \times 10^{10}$	1	4.7	$(5.2 \pm 0.24) \times 10^9$
6. $COO^-_B + H^+$	1	4.5	$(3.0 \pm 0.3) \times 10^9$	1	4.5	$(5.0 \pm 0.4) \times 10^9$
7. $Flu^- + COOH_A$			$\mathbf{(3.5 \pm 0.4) \times 10^{10}}$			$\mathbf{(1.5 \pm 0.5) \times 10^{10}}$
8. $Flu^- + COOH_B$			$(5.0 \pm 2.0) \times 10^9$			$(5.0 \pm 0.5) \times 10^9$
9. $\Phi O^- + COOH_0$			$k \leq 1.0 \times 10^7$			$k \leq 1.0 \times 10^7$
10. $\Phi O^- + COOH_0$			$k \leq 1.0 \times 10^7$			$k \leq 1.0 \times 10^7$
11. $\Phi O^- + COOH_A$			$k \leq 1.0 \times 10^7$			$k \leq 1.0 \times 10^7$
12. $\Phi O^- + COOH_B$			$k \leq 1.0 \times 10^7$			$k \leq 1.0 \times 10^7$
13. $\Phi O^- + FluH$			$\mathbf{(3.2 \pm 0.3) \times 10^8}$			$\mathbf{(1.5 \pm 0.1) \times 10^8}$
14. $COOH_A + COO^-_B$			$(1.5 \pm 0.8) \times 10^8$			$(1.0 \pm 0.8) \times 10^8$

[a] COO^-_0 (reaction 4) represents the carboxylates on the unlabeled protein and consists of 58% and 41% of the total buffer capacity of the BO_{36} and the BO_{38}, respectively. The p*K* of these groups is an average value.

the fluorescein occurs not only by reaction of the dye with free protons but that a fair fraction of the proton pickup by the surface-bound dye is due to reshuffling of the protons among the surface groups. The continuous line, shown in the figure, that follows the experimental transient within the level of the electronic noise is the numeric reconstruction of the reaction.

The observed tracings of either the BO or the BR preparations were simulated by numeric integration of the differential rate equations that correspond with the experimental system using the model defined in Scheme 1.

The proton transfer reactions in the scheme fall into two categories: one is the second-order diffusion-controlled reactions of the free protons and the free pyranine anion with the protein bound reactants. In the other category are the reactions having virtual second-order rate constants for the exchange of proton among the surface groups. The magnitude of the virtual rates constants are useful for comparative purposes, but they have no physical meaning (*14*).

The reactions represented in Scheme 1 were linked by a set of coupled, nonlinear, differential rate equations that comply with the detailed balance principle. Numeric integration of the equations with the appropriate rate constants, which are introduced as adjustable parameters, reproduced the observed signals. The continuous smooth curves shown in the figures that follow were reconstructed by this procedure.

Table 2 lists the p*K* values and the kinetic parameters of the carboxylic moieties on the two sides of the BO membranes and their relative content with respect to the protein molecule. The parameters that significantly differ between the two preparations are printed in bold letters. Just as in wild type BO protein (*15*) the two BO preparations used in the present study exhibit only one proton-binding site on the EC face of the membrane (COO^-_{EC}) and two carboxylates on its CP face. Each of the kinetically discernible proton-binding site has its own thermodynamic and kinetic characteristics.

The BO preparations are characterized by two carboxylates on the CP surface of the protein. One of them, marked as COO^-_B (see Table 2, line 6), has a p*K* of 4.5 and reacts with free protons at a rate (3×10^9 M^{-1} s^{-1}) that is slower than a diffusion-controlled reaction. Because both BO_{36} and BO_{38} exhibit one carboxylate with similar properties, it is assumed to be the same in both of the two BO preparations. The second carboxylate COO^-_A is located very close to the fluorescein-binding site; the virtual second-order rate of proton transfer from the A type carboxylate to the dye (see Table 2, line 7) is larger than 10^{10} M^{-1} s^{-1}. The A type carboxylates in the two preparations are not identical; they differ both in their p*K*s and in their rates of protonation (line 5). The BO_{38} protein has an A type carboxylate with a lower p*K* and a slower rate of reaction with free protons than does BO_{36}. The difference between the preparations is a consequence of the amino acid sequence. The BO_{38} retains its D36 moiety while BO_{36} has the D38 as the nearby carboxylate. On the basis of these observations we identify the carboxylate next to the fluorescein at the 36th position as D38 and that close to the fluorescein label on BO_{38} as D36.

The reactivity of the fluorescein moiety varies with the site of attachment. Both of the free diffusing ions, proton (line 2 in Table 2) and or pyranine (line 13 in Table 2), exhibit faster reaction with the dye when attached to the exposed 36th residue rather than when bound at the orifice of the channel (position 38).

The BO preparations are a simple model for the study of the dynamics of bulk to surface proton transfer: the protein is photo-inactive, and the number of proton binding sites is small. However, the analysis of this system facilitated the investigation of the more complex system, BR preparations.

Protonation of Surface Groups of Labeled Bacteriorhodopsin

The measurements of pulse protonation of the photoreactive BR preparation calls for discrimination between protonation of the fluorescein driven by the discharge of protons from the pyranine molecule and those released by the BR itself. For this reasons all observations were made as depicted in Figure 3.

Figure 3A depicts the transients as measured with BR_{36} preparation in the absence of pyranine. The top tracing was measured at 458 nm, while the bottom curve was monitored at 496 nm. Under these conditions the only source for protons is the light-driven photocycle of the protein. Accordingly, the 458 nm trace corresponds to minor contribution of the photocycle intermediates while the protonation of the fluorescein is slow and marginal in size. Comparable signals were measured by other groups (*9*, *20*, *25*−*27*). The

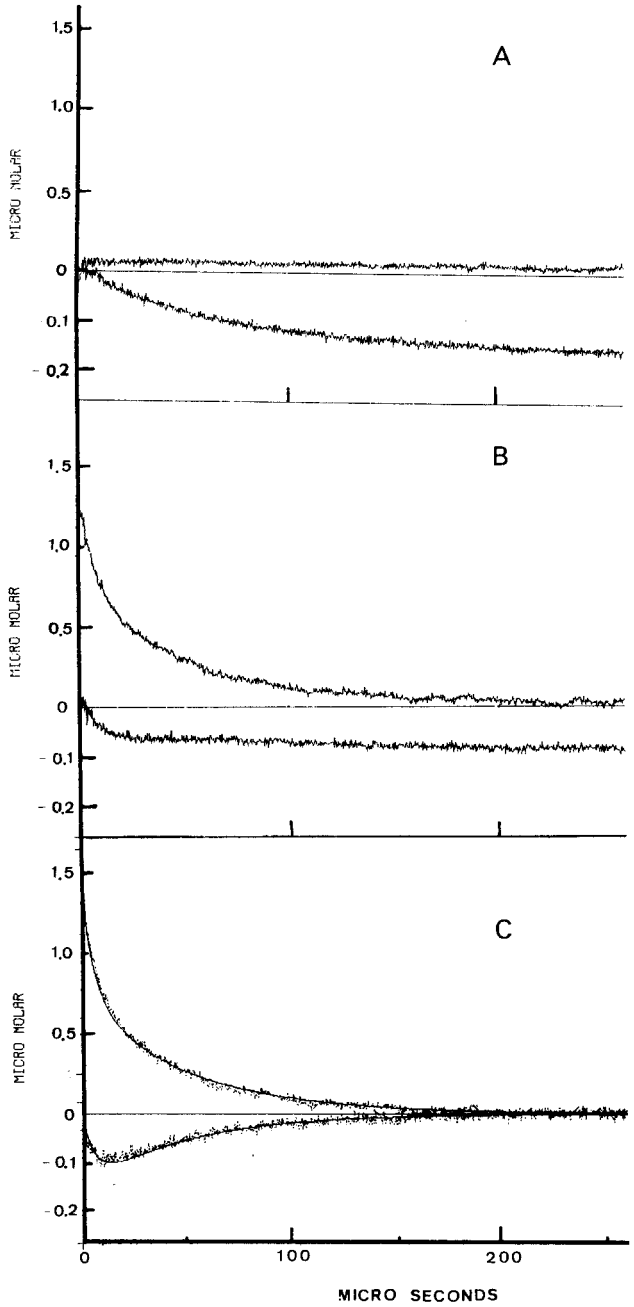

FIGURE 3: Kinetics of protonation of fluorescein attached to BR at residue 36. The protein 19.45 μM, containing 8.17 μM bound fluorescein, was suspended in 1 mM NaCl at pH = 7.4. (A) Transients measured at 458 nm (top) and at 496 nm (bottom). (B) The same kinetics after addition of 24 μM pyranine. (C) Product of vector subtraction of the transients in B minus those in A. The continuous line in C is the numeric reconstruction of the observed signals using the parameters listed in Table 3. For clarity, the fluorescein signals, depicted at the lower parts of the figure, are drawn on an expanded scale.

signals in Figure 3B were measured with pyranine as a proton source. In this case, the ΦO^- signal (top trace) is large and the fluorescein protonation (bottom curve) is much faster. On subtraction of the transients in Figure 3A from those given in Figure 3B we obtained the protonation of the fluorescein by the protons released from the pyranine. The shape of the curve is similar in size and in temporal characteristics to that recorded with the photo-inactive BO preparation. The continuous line in Figure 3C is the reconstructed dynamics using the kinetic and equilibrium parameters listed in Table 3. The parameters that significantly differ between the two preparations are printed in bold letters.

The kinetic measurements as shown in Figure 3 were carried out with BR_{38} and the result of a typical experiment together with the fitted dynamics is shown in Figure 4. These experiments with both BR preparations were carried out in the pH range 7.1−8.5, and each was simulated by a single set of adjustable parameters. In accordance with the higher charge density on the CP surface of the native protein (Table 1) and its higher buffer capacity (*15*), the simulation of the dynamics necessitated a larger number of carboxylates on the CP surface. The minimal number of carboxylates was found to be five, having nonidentical p*K* and kinetic rate constants. The p*K* values, the stoichiometric relation between the reactants, and the rate constants required to reconstruct the measured transients are given in Table 3.

The two preparations are characterized by a cluster of three carboxylates (COO^-_C) having a fast rate of reaction with free protons and a relatively high p*K* (see line 7 in Table 3). There are also two carboxylates, COO^-_A and COO^-_B, which differ from each other in their p*K*, rates of proton binding, and rates of proton exchange with the fluorescein (lines 5, 6, 8, and 9 in Table 3). The A type carboxylate exchanges proton with the fluorescein at an extremely fast rate (2×10^{12} M^{-1} s^{-1}). This group is identified as the carboxylate adjacent to the dye (D36 and D38 for the BR_{38} and BR_{36}, respectively). The second carboxylate (COO^-_B) is of the remote type like the one identified for the BO preparations (see Table 2).

DISCUSSION

Effect of the Protein on the Rate of Protonation of the Bound Indicator

The experimental curves measured under the various initial conditions (pH, reactant concentrations, and magnitude of the perturbing pulse) appear to be similar in shape. Consequently, to demonstrate that each preparation follows its own dynamics it is necessary to execute the measurements under identical conditions, which is technically impossible. On the other hand, the numeric simulation can easily reproduce a "virtual experiment" where all of the empirical conditions are identical while the kinetic and thermodynamic parameters were as determined for each of the different preparations. These calculations are shown in Figure 5. Figure 5A represents the signals reconstructed for the retinal-devoid membranes, while Figure 5B was calculated for the BR preparations. From the top curves of each frame, which represent the reprotonation of the pyranine anion, we evaluate the buffering property of the sample; the larger the buffer capacity, the slower the observed relaxation. The exchange of protons among the surface groups can be derived from the shape and amplitude of the fluorescein signal (bottom curves in Figure 5). Faster protonation implies that the surface carboxylates are assist in the transfer of protons to the fluorescein. As clearly demonstrated by the shape of the curves, the dynamics are characteristic for each preparation. The faster relaxation of the ΦO^- signal in the BO_{38} sample indicates that its buffer capacity is smaller than that of BO_{36}. In parallel, the protonation of the BO_{38} fluorescein is less extensive than that bound to the more exposed 36th residue. The fluorescein curves shown in Figure 5A

Table 3: Kinetic and Thermodynamic Characterization of the Fluorescein and the Carboxylates on the Cytoplasmic Surface of the Bacteriorhodopsin[a]

	Flu−BR_{36}			Flu−BR_{38}		
reaction	*n*	p*K*	*k*	*n*	p*K*	*k*
1. $\Phi O^- + H^+$			$(3.5 \pm 2.8) \times 10^{10}$			$(3.4 \pm 0.9) \times 10^{10}$
2. $Flu^- + H^+$			$\mathbf{(4.2 \pm 0.7) \times 10^{10}}$			$\mathbf{(1.0 \pm 0.7) \times 10^{10}}$
3. $COO^-_{EC} + H^+$	1	5.1	$(1.0 \pm 0.5) \times 10^9$	1	5.1	$(1.0 \pm 0.5) \times 10^9$
4. $COO^-_0 + H^+$	5	4.7	$(5.0 \pm 0.1) \times 10^{10}$	5	4.7	$(5.0 \pm 0.5) \times 10^{10}$
5. $COO^-_A + H^+$	1	4.8	$(1.8 \pm 0.5) \times 10^{10}$	1	4.5	$(3.0 \pm 0.5) \times 10^{10}$
6. $COO^-_B + H^+$	1	5.1	$(1.0 \pm 1.1) \times 10^{10}$	1	5.1	$(1.0 \pm 0.5) \times 10^{10}$
7. $COO^-C + H^+$	3	5.7	$\mathbf{(2.6 \pm 1.1) \times 10^{10}}$	3	5.7	$\mathbf{(5.8 \pm 0.9) \times 10^{10}}$
8. $Flu^- + COOH_A$			$(2.18 \pm 1.12) \times 10^{12}$			$(2.05 \pm 1.1) \times 10^{12}$
9. $Flu^- + COOH_B$			$(5.0 \pm 0.5) \times 10^6$			$(1.0 \pm 0.5) \times 10^6$
10. $Flu^- + COOH_C$			$(1.0 \pm 0.5) \times 10^6$			$(1.28 \pm 0.17) \times 10^{10}$
11. $\Phi O^- + FluH$			$\mathbf{(2.1 \pm 0.1) \times 10^8}$			$\mathbf{(10.4 \pm 0.3) \times 10^8}$
12. $\Phi O^- + COOH_{EC}$			$k \leq 1.0 \cdot 10^7$			5.0×10^8
13. $\Phi O^- + COOH_0$			$k \leq 1.0 \times 10^7$			1.7×10^9
14. $\Phi O^- + COOH_A$			$k \leq 1.0 \times 10^7$			1.0×10^8
15. $\Phi O^- + COOH_B$			$k \leq 1.0 \times 10^7$			1.0×10^6
16. ΦO^- $COOH_C$			5.0×10^8			$(1.58 \pm 0.05) \times 10^9$
17. $COO^-_B + COOH_C$			$k \leq 1.0 \times 10^7$			$k \leq 1.0 \times 10^6$
18. $COO^-_C + COOH_A$			$k \leq 1.0 \times 10^7$			$k \leq 5.0 \times 10^8$
19. $COO^-_A + COOH_B$			$k \leq 1.0 \times 10^6$			$k \leq 1.0 \times 10^6$

[a] COO^-_0 (reaction 4) represents the carboxylates on the unlabeled protein and consists of 58% and 65% of the total buffer capacity of the BR_{36} and the BR_{38}, respectively. The p*K* of these groups is an average value.

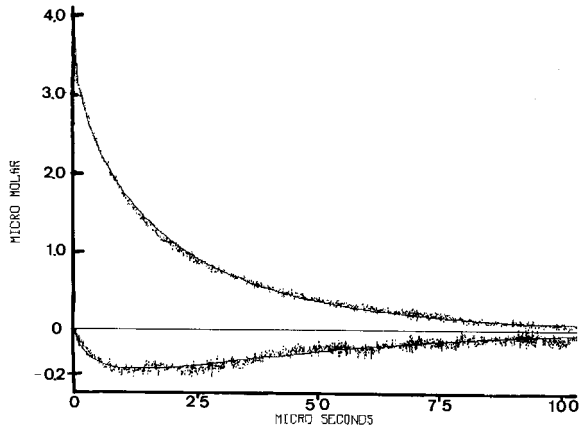

FIGURE 4: Kinetics of protonation of fluorescein attached to BR at residue 38. The measurements were carried out as described in Figure 3 using 9.24 μM of the protein containing 3.2 μM bound fluorescein in the presence of 20 μM pyranine at pH = 7.4. For clarity, the fluorescein signal, depicted at the lower part of the figure, is drawn on an expanded scale.

demonstrate that the proton-binding dynamics of the very same molecule are a function of its local environment, and a minor shift in its point of attachment is sufficient to alter the whole profile of its dynamics.

The different pattern seen in Figure 5B, depicts the dynamics of the BR preparations. The top curves imply that BR_{38} has a higher buffer capacity than the BR_{36}. Examination of the fluorescein signals reveals that the dye at the 38th residue, the orifice of the protonic channel, is more intensively protonated than that attached to the more exposed 36th position. The enhanced protonation of the indicator attached to the orifice implies that the proton entry to the channel is not only due to reaction with bulk protons but that it is heavily assisted by the funneling of protons on the surface of the protein.

Quantitative Evaluation of the Rate Constants

1. Reactions with the Fluorescein. The fluorescein moiety on the protein participates in diffusion-controlled reactions with two ions: the free proton and the $Z = -4$ pyranine anion. The reaction with proton is faster when the dye is attached to the BR at the 36th position than at the 38th one (4.2×10^{10} vs 1×10^{10} M^{-1} s^{-1}, respectively). Such a difference can be due to local electric charges and/or variation in its exposure to the bulk. The rate of collisional deprotonation of the fluorescein by the free diffusing pyranine anion is faster with the BR_{38} than with the 36th adduct (compare lines 2 and 11 in Table 3). The apparent discrepancy between the rates of reaction with the two free ions suggests the presence of an electric potential that affects the accessibility of the ions according to their charge.

The rate constants for the protonation of the fluorescein on the CP surface of the BO preparations are significantly smaller ($\sim 5 \times 10^9$ M^{-1} s^{-1}) than those measured for the BR. This finding, together with the reduction in the number of exposed carboxylates, suggests that the removal of the retinal distorts the structure of the protein.

2. Reactivity of the Carboxylates with the Bulk. Both BR_{36} and BR_{38} have five carboxylates on their CP side of the membrane that differ in their kinetic and thermodynamic properties. The protein labeled on the 38th position has one cluster of three carboxylates (COO^-_C) characterized by p*K* = 5.7, which is a rather high value for carboxylates that are exposed on the surface. The rate of protonation of each residue in the cluster (5.8×10^{10} M^{-1} s^{-1}) is faster than the rate of protonation of the free diffusing pyranine anion. To attain such a fast rate the negative charges of the carboxylates must be placed sufficiently close so that their Coulomb cages will merge to generate a common proton attractive site (*15*, *28*). On the basis of the high p*K* value and the unusual rate constant of their proton binding, we define the three carboxylates as a functional cluster.

The two other carboxylates of the CP surface of the BR_{38} are well distinguished from each other. The major difference is in their rate of proton exchange with the fluorescein. The A type carboxylate delivers its proton to the fluorescein with a virtual second-order rate constant of 2×10^{12} M^{-1} s^{-1}, (line 8, Table 3), indicating a very close proximity between

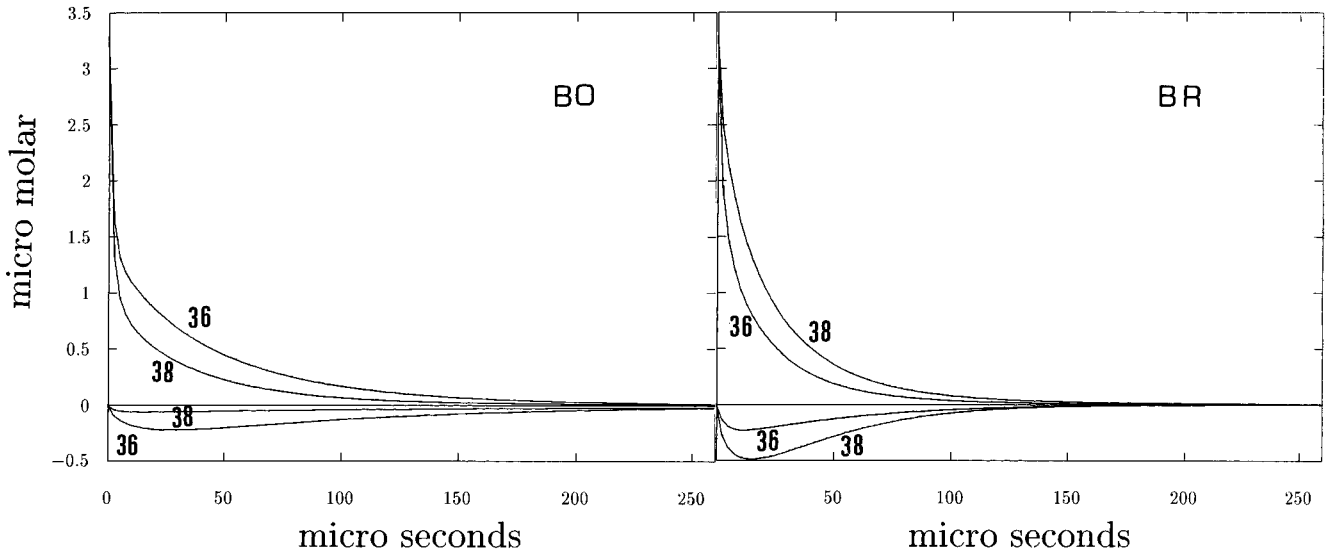

FIGURE 5: Comparison of the proton pulse dynamics of the four studied preparations. The curves are the output of a virtual experiment in which the initial conditions of the four systems are identical (9.24 μM protein containing 3.2 μM bound fluorescein, at pH = 7.2, in the presence of 20.0 μM pyranine). At zero time, 3.3 μM of the pyranine was dissociated and the resulting reactions between the reactants were calculated with the appropriate parameters listed for each preparation in Tables 2 and 3. The fluorescein signals and their simulated curves are drawn on an expanded scale.

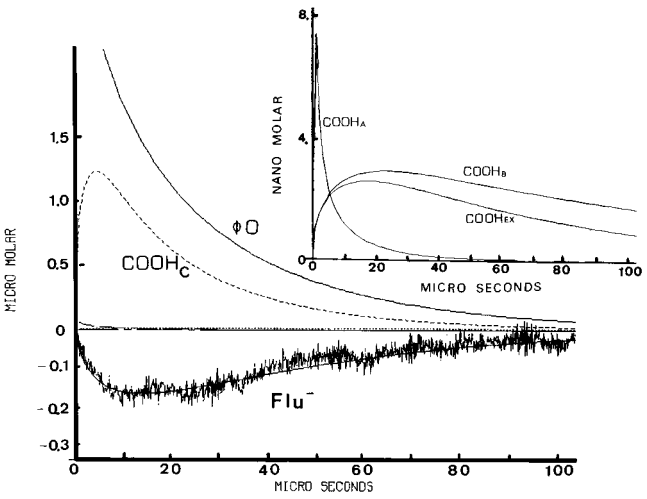

FIGURE 6: Kinetic simulation of the partial reaction involved in proton transfer to BR_{38} by protons released in the bulk. The main frame depicts the transient of the pyranine anion (ΦO^-), the C type carboxylates ($COOH_C$), and the fluorescein anion (Flu^-). The fluorescein signal together with its experimental signal are drawn on an expanded scale. The inset shows the protonation dynamics of the A type ($COOH_A$), B type ($COOH_B$) and the extracellular ($COOH_{EC}$) carboxylates. The simulations are the same as for the sample described in the legend to Figure 4 except that the pH was 8.0.

the donor and acceptor sites. This group has a low p*K* (4.7) and a fast reaction with free proton. The A type carboxylate moieties, as in the BO samples, can be identified as D38 and D36 for the BR_{36} and BR_{38}, respectively.

The second carboxylate (COO^-_B) has a slower rate of protonation and is rather remote from the orifice of the protonic channel (line 9, Table 3).

Comparison of the pyranine dynamics of the two BR preparations indicate that the BR_{38} has a larger buffer capacity (see Figure 5). The binding of the fluorescein at the 36th position changes the pattern of the reactive carboxylates. The highly reactive cluster of BR_{36} has lost some of its proton attractivity and its rate of proton binding is reduced to 2.6×10^{10} M^{-1} s^{-1}. The lower rate implies that the residues making the cluster are less compact.

3. Proton Transfer between the Surface Groups. The virtual rate constants of proton exchange between the A type carboxylate and the fluorescein on the CP surface are extremely fast reactions that exceed those measured for micellar systems or fluorescein bound to bovine serum albumin (*18*, *21*). Comparable rates were measured only for proton transfer within the heme binding site of apomyoglobin (*29*) or between sites located on small molecules such as dicarboxy fluorescein (*31*). The proton transfer from the C type cluster to the fluorescein is also of a significant rate, indicating that the cluster is sufficiently close to the fluorescein to sustain a rapid, efficient proton transfer among them. The combined reactions of the A and the C type carboxylates with bulk protons provide the surface of the CP side of the membrane with an effective proton-collecting antenna.

The B type carboxylate is operatively disconnected from the proton-collecting antenna. The measured rates imply that the transfer of the proton from the B carboxylate to the fluorescein proceeds only after dispersion of the proton to the bulk.

Detailed Mechanism of Proton Transfer to the Orifice of the Channel

The protonation of fluorescein on residue 38 is a sum of many parallel reactions in which all groups of the surface are involved. The detailed dynamics of each moiety is drawn in Figure 6. The dynamics of the three carboxylates are marked as $COOH_C$. Its initial rate of protonation is fast: it gathers some 30% of the released protons and retains them over a period of almost 50 μs. All other reactants exhibit much smaller signals, and their dynamics are expanded in the inset to the figure. Of the three moieties shown in the inset, the one corresponding with the A type carboxylate (D36) has a very distinctive feature ($COOH_A$). Its initial protonation is very fast, almost as rapid as that of the cluster, yet within the time frame of a microsecond, its dynamics reverses its direction and the loss of the proton coincides

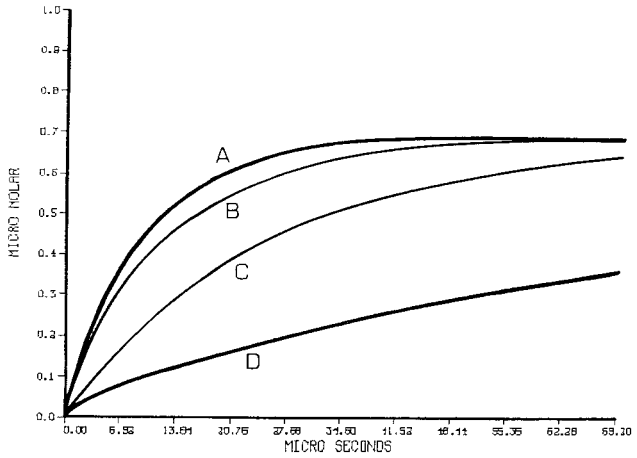

FIGURE 7: Simulation of the dynamics of protonation of the fluorescein bound on residue 38 under virtual conditions of a step function perturbation by 3.3 μM H^+ released in the bulk. Curve A depicts the dynamics when all surface carboxylates participate in proton binding and delivery. In curve B the three carboxylates cluster is inoperative in proton transfer to the fluorescein. Curve C is calculated when the A type carboxylic acid does not deliver its proton to the fluorescein. Curve D is calculated when all proton transfer reactions between the surface groups are eliminated. The calculations were carried out for the sample described in the legend to Figure 4 at pH = 7.5.

with the protonation of the fluorescein. The other two carboxylates drawn in the inset are the one on the EC surface (*15*) and the slow-reacting one (type B) on the CP face. Their dynamics look uncoupled with that of the fluorescein or of the other moieties.

To demonstrate the efficiency of the proton delivery system we simulated in Figure 7 the scenario which approximats the function of the BR under a step function perturbation. The initiation of the reaction in this figure is by instantaneous generation of 3.3 μM H^+ in the bulk of the solution, and their accumulation on the fluorescein at residue 38 is taken to represent their entrance to the channel. Curve A depicts the dynamics when all proton transfer reactions are active, as determined for the BR_{38} membranes. Curve B reproduces the dynamics under the hypothetical situation that the cluster does not deliver its proton to the channel. The calculated reaction is appreciably slower. Blocking the transfer of protons from D38 to the channel (curve C) almost halves the initial velocity of the reaction. Finally, Curve D was calculated when neither the cluster nor D36 were funneling proton to the channel; the velocity is much slower, even less then the sum of the decrements as in curve B plus C.

The results of our measurements, and the corresponding analysis indicate that the passage of protons from the bulk to the orifice of the CP protonic channel is assisted by the surface carboxylates. The cluster acts as a primary acceptor. The combination of its relative high p*K* and extremely fast reaction with bulk protons renders it an effective competitor for the bulk protons. For this reason the CP surface of BR has the kinetic competence to pick up protons from the well-buffered cytoplasmic matrix. The release of the proton from the cluster supplies a proton to the nearby carboxylate of D36, which rapidly delivers it to the channel. Indeed, replacement of the carboxylate at position 36 has a marked effect on the proton uptake by the post M state intermediates (*8*).

The presence of a proton-collecting antenna, as described above, raises the questions what are its dimensions and is it limited to the size of a single protein or does it span the entire membrane? The size of an efficient proton-collecting antenna was investigated in previous studies and deduced to be about 30 Å. These estimations were based either on a theoretical model (*12*, *14*, *28*) or on measurements with phospholipid membranes (*22*, *32*). In the present study we may have a more precise estimation that is based on the dynamics of the B type carboxylate on the CP surface, a moiety that does not assist in the protonation of the fluorescein. Thus this carboxylate is either too remote from the channel or the proton passage to the channel is obstructed by the repulsive potential of a positive surface residue that disrupts the connectivity. Whatever the mechanism, the observation itself implies that the dimension of the antenna is comparable to, or smaller than, the dimension of the bacteriorhodopsin molecule.

Finally, we wish to point out that the same conclusions which connect the structure of the CP face with its physiological functionality had been advocated by Kimura (personal communication). On the basis of the structural study Kimura et al. detect a negatively charged domain that surrounds the orifice of the channel plus a positively charged rim that encircled the perimeter of the protein. The position of that proton repulsive barrier indeed insulates one BR molecule from the others, limiting the surface of the proton-collecting antenna to be equal to or smaller than the protein's surface.

ACKNOWLEDGMENT

The authors are grateful to Dr. D. Oesterhelt from the Max Planck Institute for Biochemistry, Martinsried, Germany, for providing us the D36C and the D38C mutants of bacterial rhodopsin.

REFERENCES

1. Henderson, R., and Unwin, P. N. T. (1975) *Nature* (*London*) *257*, 28−32.
2. Henderson, R., Baldwin, J. M., Ceska, T. A., Zemlin, F., Beckmann, E., and Downing, K. H. (1990) *J. Mol. Biol. 213*, 899−929.
3. Grigorieff, N., Ceska, T. H., Downing, K. H., and Henderson, R. (1996) *J. Mol Biol. 259*, 393−421.
4. Kushwaha, S. C., Kates, M., and Martin, W. G. (1975) *Can. J. Biochem. 53*, 284−292.
5. Kates, M., Kushwaha, S. D., and Sprott, G. D. (1982) *Methods Enzymol. 88* 98−111.
6. Glaeser, R. M., Jubb, J. S., and Henderson, R. (1985) *Biophys. J. 48*, 775−780.
7. Jonas, R., Koutalos, Y., and Ebrey, T. G. (1990) *Photochem. Photobiol. 52*, 1163−1177.
8. Riesle, J., Oesterhelt, D., Dencher, N. A., and Heberle, J. (1996) *Biochemistry 35*, 6635−6642.
9. Alexeiv, U., Scherrer, P., Marti, T., Khorana, H. K., and Heyn, M. P. (1995) *FEBS Lett. 373*, 81−84.
10. Renthal, R., McMillan, K., Guerra, L., Garcia, N. M., Rangel, R., and Jen, C.-M. (1995) *Biochemistry 34*, 7869−7878.
11. Cybulski, S. M., and Scheiner, M. (1989) *J. Am. Chem. Soc. 111*, 23−31
12. Gutman, M., and Nachliel, E. (1990) *Biochim. Biophys. Acta 1015*, 391−414.
13. Scheiner, M., and Duan, X. (1991) *Biophys. J. 60*, 874−883.
14. Gutman, M., and Nachliel, E. (1997) *Annu. Rev. Phys. Chem. 48*, 323−350.
15. Nachliel, E., Gutman, M., Kiryati, S., and Dencher, N. A. (1996b) *Proc. Natl. Acad. Sci. U.S.A. 93*,10747−10752.

16. Pines, E., Huppert, D., and Agmon, N. (1988) *J. Chem. Phys. 88*, 5620−5630.
17. Gutman, M. (1986) *Methods Enzymol, 127*, 522−38.
18. Yam, R., Nachliel, E., and Gutman, M. (1988) *J. Am. Chem. Soc. 11*, 2636−2640.
19. Ferrando, E., Schweiger, U., and Oesterhelt, D. (1993) *Gene 125*, 41−47.
20. Heberle, J., Risele, J., Thiedemann, G., Oesternhelt, D., and Dencher, N. A. (1994) *Nature 370*, 379.
21. Gutman, M. (1984) *Methods Biochem. Anal. 30*, 1−103.
22. Nachliel, E., Finkelstein, Y., and Gutman, M. (1996a) *Biochim. Biophys. Acta* 1285, 131−145.
23. Ehrenberg, E., Ebrey, T. G., Friedman, N., and Sheves, M. (1989) *FEBS Lett. 250*, 179−183.
24. Nachliel, E., and Gutman, M. (1996) *FEBS Lett. 393*, 221−225.
25. Heberle, J., and Dencher, N. A. (1990) *FEBS Lett. 277*, 277−280.
26. Alexiev, U., Mollaaghababa, R., Scherrer, P., Khorana, H. G., and Heyn, M. P. (1995a) *Proc. Natl. Acad. Sci. U.S.A. 92*, 372−378.
27. Cao, Y., Brown, S. L., Sasaki, J., Maeda, A., Needleman, R., and Lanyi, K. J. (1995) *Biophys. J. 68*, 1518−1530.
28. Gutman, M., Nachliel, E., and Tsfadia, Y. (1995) in *Permeability and stability of Lipid Bilayers* (Disalvo, E. A., and Simon, S. A., Eds.) pp 259−276, CRC Press, Ann Arbor, MI.
29. Shimoni, E., Tsfadia, Y., Nachliel, E., and Gutman, M. (1993) *Biophys. J. 64*, 472−479.
30. Nachliel, E., and Gutman, M. (1984) *Eur. J. Biochem. 143*, 83−88.
31. Sacks, V. (1997) M.Sc. Thesis, Tel Aviv University.
32. Bransburg-Zabary, S., Nachliel, E., and Gutman, M. (1996) *Biochim. Biophys. Acta 1285*, 146−154.

BI9717542